plant biology

Plant Biology ISSN 1435-8603

RESEARCH PAPER

Gating of the two-pore cation channel AtTPC1 in the plant vacuole is based on a single voltage-sensing domain

D. Jaślan[1,*], T. D. Mueller[1,*], D. Becker[1], J. Schultz[2], T. A. Cuin[1], I. Marten[1], I. Dreyer[3], G. Schönknecht[4] & R. Hedrich[1]

1 Institute for Molecular Plant Physiology and Biophysics, University of Würzburg, Würzburg, Germany
2 Center for Computational and Theoretical Biology, Campus Hubland Nord, Department of Bioinformatics, Biocenter, University Würzburg, Würzburg, Germany
3 Centro de Bioinformática y Simulación Molecular (CBSM), Universidad de Talca, Talca, Chile
4 Department of Plant Biology, Ecology, and Evolution, Oklahoma State University, Stillwater, OK, USA

Keywords
Arabidopsis thaliana; gating; plant TPC1; two-pore ion channel; vacuole; voltage sensor.

Correspondence
G. Schönknecht, Department of Plant Biology, Ecology, and Evolution, Oklahoma State University, Stillwater, Oklahoma 74078, USA.
E-mail: gschoen@okstate.edu
R. Hedrich, Institute for Molecular Plant Physiology and Biophysics, University of Würzburg, Julius-von-Sachs Platz 2, D-97082 Würzburg, Germany.
E-mail: hedrich@botanik.uni-wuerzburg.de

*These authors contributed equally to this work.

Editor
H. Rennenberg

Received: 3 June 2016; Accepted: 6 June 2016

doi:10.1111/plb.12478

ABSTRACT

- **The two-pore cation channel TPC1 operates as a dimeric channel in animal and plant endomembranes. Each subunit consists of two homologous Shaker-like halves, with 12 transmembrane domains in total (S1–S6, S7–S12). In plants, TPC1 channels reside in the vacuolar membrane, and upon voltage stimulation, give rise to the well-known slow-activating SV currents.**
- **Here, we combined bioinformatics, structure modelling, site-directed mutagenesis, and in planta patch clamp studies to elucidate the molecular mechanisms of voltage-dependent channel gating in TPC1 in its native plant background.**
- **Structure-function analysis of the Arabidopsis TPC1 channel in planta confirmed that helix S10 operates as the major voltage-sensing site, with Glu450 and Glu478 identified as possible ion-pair partners for voltage-sensing Arg537. The contribution of helix S4 to voltage sensing was found to be negligible. Several conserved negative residues on the luminal site contribute to calcium binding, stabilizing the closed channel.**
- **During evolution of plant TPC1s from two separate Shaker-like domains, the voltage-sensing function in the N-terminal Shaker-unit (S1–S4) vanished.**

INTRODUCTION

In the 1980s, patch clamp studies on plant vacuoles identified a calcium-dependent slow-activating ion channel, the SV channel (Hedrich *et al.* 1986; Hedrich & Neher 1987). The SV channel of the model plant *Arabidopsis thaliana* is a non-selective cation channel, equally permeable to K^+ and Na^+ (Ivashikina & Hedrich 2005; Ranf *et al.* 2008). About 20 years after the discovery of SV channel currents, Peiter *et al.* (2005) demonstrated that the *Arabidopsis* SV channel is the gene product of *AtTPC1*. In plants, a single *TPC1* gene has been described in *Arabidopsis* and most other higher plants (Hedrich & Marten 2011), and in rice, it has been confirmed that the SV channel is synonymous to OsTPC1 (Dadacz-Narloch *et al.* 2013). The first *TPC* genes were cloned from rat by Ishibashi *et al.* (2000) and from *Arabidopsis* by Furuichi *et al.* (2001). As with the plant TPCs, animal homologues localise to the endolysosomal compartment (Wang *et al.* 2012; Cang *et al.* 2014).

Two-pore cation channels (TPCs) belong to the large superfamily of voltage-gated ion channels that have evolved three related topologies. (i) Single voltage-domain channels, *e.g.* K^+ channels and bacterial Na^+ channels, assemble from four separate, often identical, Shaker-like domains. (ii) In four-domain channels represented by the eukaryotic Ca^{2+}/Na^+ channels, four homologous Shaker-like domains are fused and a single amino acid chain forms the transmembrane protein. (iii) TPCs with two concatenated Shaker-domains (D1 and D2; Fig. 1, inset), which form functional channels as dimers, can be regarded as an evolutionary intermediate between one- and four-domain voltage-gated ion channels (Rahman *et al.* 2014). Plant TPCs share sequence similarity with their animal counterparts (up to 30% amino acid identity and 50% similarity), and animal and plant TPCs probably have functional properties in common, whilst also exhibiting differences. In contrast to animals, plant TPC1s have evolved a cytosolic calcium-binding double EF-hand linker region, connecting the two Shaker-like domains (Peiter *et al.* 2005; Schulze *et al.*

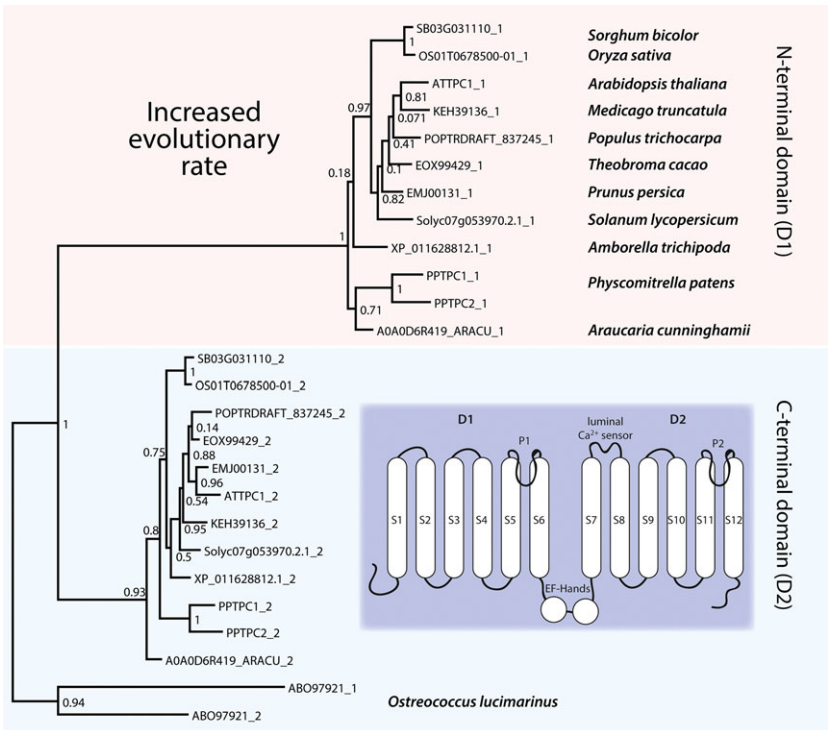

Fig. 1. Phylogenetic tree of the N- and C-terminal ion transport domains of selected plant TPC1 sequences. *Ostreococcus lucimarinus* was selected as an outgroup for rooting. The longer branch at the base of D1 indicates an increased evolutionary rate compared to the rest of the tree ($P < 0.001$). Inset: Linear topology model of plant TPC1 proteins depicting the N-terminal (D1; transmembrane regions S1–S6) and C-terminal (D2; transmembrane regions S7–S12) domains that are connected by a cytosolic calcium-binding EF-hand domain. The calcium sensor exposed to the vacuolar lumen locates in the S7–S8 linker region.

2011). Calcium binding to EF-hand 2 promotes channel opening by shifting the voltage dependence to less positive, more physiological membrane potentials (Hedrich & Neher 1987; Schulze *et al.* 2011). A luminal calcium sensor has also been identified in plant TPCs (Dadacz-Narloch *et al.* 2011), although luminal calcium binding prevents channel opening by shifting the voltage dependence to more positive, less physiological membrane potentials (Pottosin *et al.* 1997, 2004). The luminal calcium-binding site is localised in the linker region between S7 and S8 (Fig. 1, inset), and appears functionally linked to the voltage sensor of TPC1. The sensitivity of the vacuolar cation channel to cytosolic and vacuolar calcium (Hedrich & Neher 1987; Pottosin *et al.* 1997) alongside the involvement of TPC1 in long-distance communication (Choi *et al.* 2014; Kiep *et al.* 2015) suggests that calcium-regulated slow vacuolar (SV) currents in plants could be involved in the transmission and amplification of stimulus-related calcium signals. Apparently, TPC1 is part of a sensory network that rapidly transmits information between distant sites in the plant body.

Here, we investigated the structural determinants of voltage- and calcium-dependent channel gating of AtTPC1. A three-dimensional homology model of AtTPC1, based on the bacterial voltage-gated Na^+ channel Na_vAb (Payandeh *et al.* 2011), was built to guide the generation of channel mutants. These mutations were not limited to positively charged residues in S4 and S10; putative ion-pair partners predicted to interact with voltage-sensing residues were also investigated. While we were finalising our analyses, the crystal structure of AtTPC1 was published (Guo *et al.* 2016; Kintzer & Stroud 2016), together with the electrophysiological characterisation of several mutants affecting voltage gating or Ca^{2+} binding (Guo *et al.* 2016). Guo *et al.* (2016) used HEK cells as a heterologous expression system for AtTPC1. We characterised our comprehensive set of mutants in a homologous expression system, *i.e. Arabidopsis* protoplasts, under more physiological conditions, thus providing insights into the structure–function relationships of AtTPC1 in its native membrane.

MATERIAL AND METHODS

Evolutionary analyses

Protein sequences containing two ion channel domains, as identified with Pfam, were extracted from selected key plant species (Finn *et al.* 2014; PF00520; Supporting Information Notes S1). The position of the domains was delineated using HMMer2 for global alignment based on the Pfam seed alignment. Domain sequences were extracted and aligned using MUSCLE (Edgar 2004). Based on this alignment, a phylogenetic tree was calculated using PhyML (Dereeper *et al.* 2008), with the robustness of the nodes estimated using the approximate likelihood ratio test (Anisimova & Gascuel 2006). Different evolutionary scenarios were tested against the topology of the resulting tree. Models that allowed only a single evolutionary rate (null hypothesis) were compared with those enabling a different rate at either the base of D1 or for the whole D1 branch, respectively. Data were fitted to these models using

codeml of the PAML package (Yang 2007). To estimate any significance, the log likelihood of the data under the single rate model was compared with that of the more complex model. As these models are nested and deviate in a single degree of freedom, the doubled difference of the log likelihood needs to be larger than the corresponding value of the chi2 distribution (2x (lnL2 – lnL1) > chi2) at the chosen significance level ($P = 0.001$) to reject the null hypothesis, *i.e.* the simple model. To identify specificity determining sites (SDPs), the out-group was deleted and domain sequences re-aligned (Fig. S1). The resulting alignment was used as the input for SDPfox (Mazin *et al.* 2010).

Plant growth and protoplast transformation with TPC1 channel constructs

The TPC1 loss-of-function mutant *Arabidopsis thaliana* (L.) Heynh. plants *tpc1-2* (Peiter *et al.* 2005) were cultivated on soil in a growth chamber under controlled short-day conditions: 8 h/16 h photoperiod at a photon flux density of 150 $\mu mol \cdot m^{-2} \cdot s^{-1}$, and a temperature of 22/16 °C. Wild-type and mutant TPC1 channel constructs fused at the C-terminus to GFP were generated following a modified USER fusion method (Nørholm 2010) as previously described (Dadacz-Narloch *et al.* 2013). Primer sequences used for introducing the point mutations into *TPC1* cDNA are listed in Table S1. The different channel constructs were transiently expressed in mesophyll protoplasts from 6- to 7-week-old *tpc1-2* plants according to Sheen (2002) and Yoo *et al.* (2007). To visualise channel expression and localisation to the vacuolar membrane, fluorescence images were taken from vacuoles hypo-osmotically released from transformed protoplasts 24 or 48 h after transformation (Fig. S2). For imaging, a ×40 Plan-Apochromat water immersion objective was used for confocal laser scanning microscopy (LSM 5 Pascal; Zeiss, Oberkochen, Germany).

Patch clamp experiments

The whole-vacuole patch clamp configuration was established on vacuoles liberated from mesophyll protoplasts 48 h after transient transformation, as previously described (Beyhl *et al.* 2009; Dadacz-Narloch *et al.* 2013). Macroscopic current recordings were performed at a sampling rate of 100 µs and low-pass filtered at 2.9 kHz using an EPC9 patch clamp amplifier (HEKA Electronic, Lambrecht, Germany). From a holding potential of −60 mV, voltage pulses ranging from −100 to +110 mV were applied in 15-mV steps. For some slow-activating mutants (R540M, R543M and R552M), the voltage pulse duration was increased from 1200 ms to 1500 ms (cf. Fig. S2). The standard bathing solution facing the cytosolic side of the vacuolar membrane contained 150 mM KCl, 1 mM $CaCl_2$ and 2 mM DTT, adjusted to pH 7.5 with 10 mM HEPES/TRIS and to an osmolality of 310 $mOsmol \cdot kg^{-1}$ with D-sorbitol. The standard pipette solution applied to the vacuolar side of the membrane comprised 150 mM KCl, 2 mM DTT, 0.1 mM EGTA, 2 mM $MgCl_2$ (no $CaCl_2$ added), adjusted to pH 7.5 with 10 mM HEPES/TRIS, with an osmolality of 310 or 400 $mOsmol \cdot kg^{-1}$ using D-sorbitol. We opted for symmetric pH to prevent a shift in voltage-dependent channel activation to more positive potentials. In experiments labelled with the extension '_10', the patch pipette solution contained 10 mM Ca^{2+} instead of EGTA. Details of the analysis of whole-vacuole currents are given in Methods S1.

Modelling the voltage sensor of TPC1

A homology model of AtTPC1 was built using the structure of the bacterial voltage-gated sodium channel Na_vAb from *Arcobacter butzleri* (PDB entry 3RV0; Payandeh *et al.* 2011). This allowed us to obtain a model for structure–function analyses of the voltage sensor(s). In contrast to the ion channel Na_vAb, which is a homo-tetramer built from four identical subunits, AtTPC1 is a dimer in which each subunit resembles the assembly of two Na_vAb monomer subunits. Thus, an amino acid sequence alignment was performed using the sequences of two Na_vAb subunits in a linear assembly and the sequence of AtTPC1 from which the plant specific EF-hand insertion was removed. The AtTPC1 monomer was then modelled using the dimeric Na_vAb assembly as present in the asymmetric unit, replacing differing amino acids using the tool ProteinDesign of the software package Quanta2008 (Accelrys, San Diego, CA, USA). Small insertions and deletions were either modelled manually, or when larger, were left truncated. Backbone torsion angles were restrained to be within the allowed region of the Ramachandran plot when possible. Excessive van der Waals contacts were eliminated by performing side chain rotamer searches using the tool Xbuilt in the software Quanta2008. The EF hand architecture was taken from the homology model (Dadacz-Narloch *et al.* 2011) and connected to the current three-dimensional model.

RESULTS

The N- and C-terminal domains of plant TPC1s evolved at different rates

To trace the evolutionary history of the *Arabidopsis* Two Pore Channel 1 protein (AtTPC1), we extracted homologues from selected key species comprising two ion channel domains, as identified with Pfam (Finn *et al.* 2014; PF00520). A phylogenetic tree resulting from an alignment of the N- and C-terminal ion transport domains (D1 and D2, respectively) revealed that both domains reliably built distinct clusters (Fig. 1). A longer branch at the base of D1, however, pointed towards increased evolutionary rates in this region. We therefore tested models that assume a single rate for the whole tree against those enabling a different rate at the base of D1 as well as for the whole D1 branch. The latter fitted the data significantly better ($P < 0.001$), indicating that the N-terminal domain D1 of TPCs evolved faster than the C-terminal domain D2 (Fig. 1). Our finding further suggests that the contribution of D1 within the TPC1 channel dimer towards voltage sensing could differ from that of D2. Hence, to identify sites involved in a possible divergence of function, we sought specificity-determining positions (SDPs) within the D1 and D2 domains that harbour different amino acids in the respective functional sub-group (Mazin *et al.* 2010; Table S1). Along with many others, we identified residues within the putative voltage-sensing regions (S4/S10) that have evolved significantly differently in D1 compared to D2 (Table S2). Amongst these, two conserved arginine residues

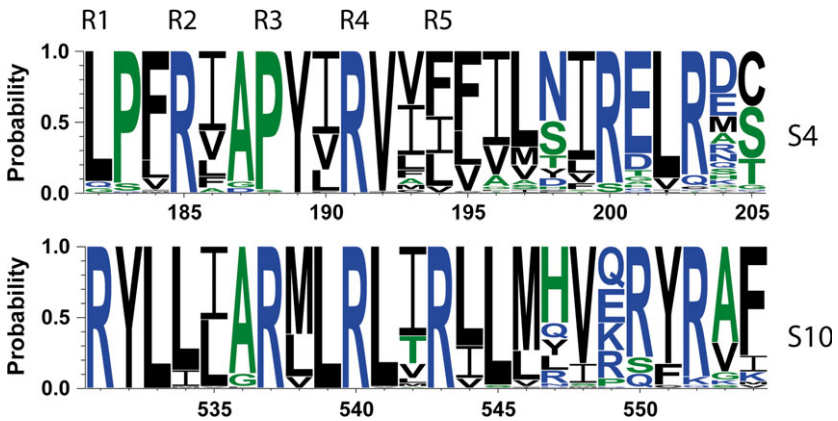

Fig. 2. Composition of transmembrane domains S4 and S10 of plant TPC1 proteins. From an alignment of 93 TPC1 proteins (Suppl. File1), sequence logos for domains S4 and S10 were generated using WebLogo 3.4 (Crooks *et al.* 2004). The probability is plotted without adjustment for amino acid composition. Numbering of amino acid residues is according to TPC1 from *Arabidopsis thaliana*. Colours indicate amino acid hydrophobicity, with blue being hydrophilic (RKDENQ), green neutral (SGHTAP) and black hydrophobic (YVMCLFIW). R1 to R5 indicate the positions of the five conserved arginine residues in a typical voltage sensor helix (Catterall 2010).

in S10, which correspond to positions Arg531 and Arg537 of AtTPC1, have evolved in S4 to leucine and proline (Leu182, Pro188, respectively; Fig. 2).

Voltage-sensing sites in the TPC1 channel protein

At the time this study was conceived, no structure data were available for the TPC1 family. Therefore, to identify promising candidates involved in voltage-sensing, we built a homology model of AtTPC1 using the crystal structure of the bacterial voltage-gated Na^+ channel Na_vAb (Payandeh *et al.* 2011). Na_vAb represented the best template available at the time, exhibiting 59% homology at amino acid sequence level, residues 1–219, to AtTPC1. One major difference is that bacterial voltage-gated Na^+ channels form homo-tetrameric arrangements that have a four-fold symmetry; TPC1 proteins form dimeric assemblies comprising two putative voltage sensors arranged in a linear tandem arrangement (Fig. 1, inset). Thus for modelling, each TPC1 subunit had to be built from two monomer subunits of the bacterial Na^+ channel. Consequently, the pore is not completely symmetrical; it consists of a dimeric arrangement with two differing pore loops. Similarly, the voltage sensor domains are built with two different transmembrane regions, S4 and S10, arranged in tandem within a single chain. A typical voltage sensor helix carries four to seven positively charged amino acid residues (usually arginine) at every third position, each separated by two hydrophobic amino acid residues (+ΨΨ+ΨΨ. . ., with Ψ indicating a hydrophobic amino acid; Catterall 2010). Four arginines arranged in such a conserved signature are present in S4 of the Na_vAb sodium channel (Catterall 2010). However, the amino acid sequence alignment (Fig. 2), as well as the analysis of the AtTPC1 3D model, indicates that the two putative voltage sensors in helices S4 and S10 differ markedly. In S4, the first arginine R1 present in the Shaker potassium channels is missing in AtTPC1, as in Na_vAb, and is replaced in AtTPC1 by leucine (Leu182). The second arginine R2 (Arg185), located in the first turn of the helix, is missing the negatively charged interaction partner present in Na_vAb (Payandeh *et al.* 2011). The third arginine, R3, is absent and replaced with a proline (Pro188). This replacement is typical for plants; all TPC1 homologues from land plants seem to carry a proline at position R2 in S4 (Fig. 2). The fourth arginine, R4, Arg191 in AtTPC1, is conserved in S4. The fifth arginine, R5, found in a typical voltage sensor helix, is missing in plant TPC1 channels. These differences suggest that helix S4 is neither a classical voltage sensor nor does it possess a voltage-sensing function.

In contrast, the signature of the second putative voltage sensor helix, S10 in AtTPC1, deviates little from a classical voltage sensor. In our model, only the second arginine R2 is not located at its assumed position in the voltage sensor helix. It is instead replaced with a conserved hydrophobic leucine residue (Leu534; Fig. 2). The three other arginine residues, Arg537, Arg540 and Arg543, occupy locations comparable to classical voltage sensor arginine residues, R3, R4 and R5. According to the 3-D homology model, the potential anchoring residues for arginine residue R3 might be Glu450 (helix S7), or alternatively, R3 could interact with Glu511 in helix S9. The third voltage-gating charge Arg540 (R4) could form a charge–charge pair with residue Asn443 or Glu468, according to the homology model. A third polar interaction partner for the R4 arginine (Arg540) might be the negatively charged glutamate residue (Glu511), which is highly conserved among plant TPC1 channels. Arg543, the fourth arginine (R5) present in AtTPC1, potentially engages with Glu478 in helix S8 and Asp500 in helix S9, forming two salt-bridge interactions. To study the contribution of the S4/S10 arginines to AtTPC1 voltage sensing, we replaced all conserved S4/S10 arginines with hydrophobic methionine and expressed the different channel mutants as GFP fusion constructs in mesophyll protoplasts from the *Arabidopsis* TPC1 loss-of-function mutant *attpc1-2*. In line with GFP-tagged TPC1 wild-type channels, GFP fluorescence confirmed expression of all S4/S10 channel mutants and their localisation in the vacuolar membrane of mesophyll cells (Fig. S2). Voltage-dependent gating characteristics of these channel mutants were studied by applying the patch clamp technique to vacuoles released from mesophyll protoplasts (Dadacz-Narloch *et al.* 2011).

The S4 arginine mutations weakly affect the voltage dependence of TPC1

Macroscopic current recordings under symmetrical K^+ buffers demonstrated that S4 mutations (R185M, R191M, R200M and R203M) did not compromise channel function (Fig. S2). TPC1 mutants activated upon depolarisation at similar voltages to wild-type channels, giving rise to comparable outward current amplitudes (Fig. 3a). Likewise, estimated half-activation times ($t_{1/2}$) of outward currents showed no significant differences in activation kinetics between wild type and any of the four S4 mutants (Fig. 3b). For quantification of potential effects of S4 arginine mutations on voltage-dependent gating characteristics, normalised macroscopic conductance–voltage curves ($G/G_{max}(V)$) were estimated from tail current measurements. Conductance–voltage curves indicated a slight shift of current activation to more positive voltages for most S4 mutants (Fig. 3c). A linear three-state model employed for SV/TPC1 channels from sugar beet and *Arabidopsis* (Pottosin *et al.* 2004; Dadacz-Narloch *et al.* 2011) was applied, and curves fitted with a Double-Boltzmann distribution, providing the two midpoint voltages for activation (V_1 and V_2) and two equivalent gating charges (z_1 and z_2). This three-state model (C2 ↔ C1 ↔ O) is composed of two closed (non-conductive) states and one open (ion-conductive) channel state, suggesting that three physical conformations exist and are consecutively passed during voltage-dependent channel opening and closing. According to the two-stage Boltzmann fit, at midpoint potential V_2, both closed states (C2 ↔ C1) are equally occupied, while at midpoint potential V_1 the closed state C1 and the open state (C1 ↔ O) are equally distributed (Methods S1; Pottosin *et al.* 2004). Furthermore, each assumed conformational transition (C2 ↔ C1, C1 ↔ O) is accompanied by the movement of charged amino acid residues within the transmembrane electrical field, reflected by the derived number of equivalent gating charges z_2 and z_1, respectively (Methods S1; Pottosin *et al.* 2004). Other than a minor positive-going shift of the voltage threshold for channel activation of R185M, R191M and R200M, as indicated by the slight increase in midpoint voltage V_1, no significant changes in voltage-dependent gating were detected in S4 mutants (Table 1, Fig. 3c). Taken together, these results suggest that arginines in S4 (Arg185, Arg191, Arg200 and Arg203) have only a minor influence on voltage-dependent gating of TPC1. This finding is consistent with our evolutionary study and the homology model, suggesting that helix S4 deviates significantly from the prototypical voltage sensor present in the bacterial Na_vAb sodium channel.

The S10 arginine mutations alter the voltage dependence of TPC1

In contrast to mutations in the S4 domain, replacement of arginine residues in the S10 domain (Fig. 2) affected current amplitudes, half-activation times and voltage-dependent gating (Fig. S2, Table 1).

Arg537, Arg540 and Arg543 are all separated by two hydrophobic residues (Fig. 2), following the conserved motif of a voltage sensor (Noda *et al.* 1984; Catterall 2010). The most pronounced effect on TPC1 gating was observed for R543M. Although GFP fluorescence proved expression of R543M channels, voltage-induced outward currents were almost undetectable from vacuoles harbouring R543M channels (Fig. S2). In contrast to R543M, R537M channels did show voltage-dependent outward currents (Fig. S2). Yet compared to wild type, R537M current densities were reduced by 70% at +110 mV (Fig. 3d), and instead of the typical multiphasic current increase, simple monoexponential current activation kinetics were observed for R537M channels. Furthermore, in contrast to wild-type channels and all other mutant channels tested, current half-activation times of R537M were voltage-independent (Fig. 3e, Table 1). Moreover, conductance–voltage curves for R537M channels could not be described with a

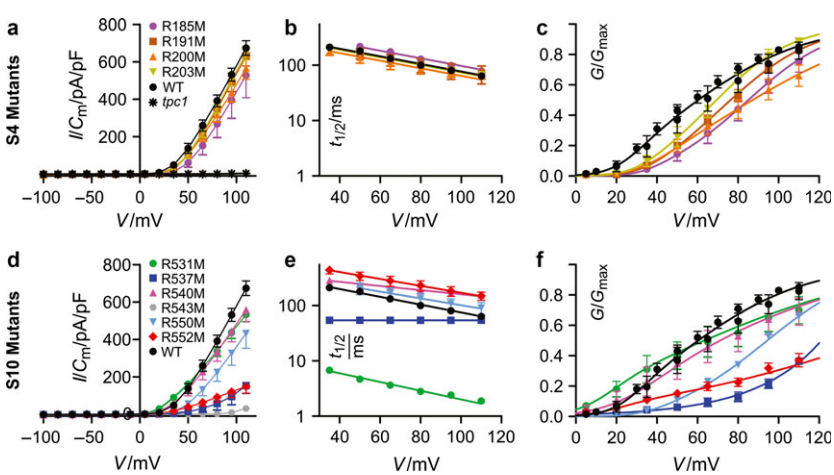

Fig. 3. Effect of mutants in domains S4 or S10 on voltage-dependent channel gating of TPC1 from *Arabidopsis thaliana*. For arginine mutations in S4 (R185M, R191M, R200M and R203M; a–c) and S10 (R531M, R537M, R540M, R543M, R550M and R552M; d–f) current amplitudes (I/C_m in pA/pF; a, d), half-activation times ($t_{1/2}$ in ms, logarithmic *y*-axis; b, e) and macroscopic conductance–voltage curves (G/G_{max}; c, f) are compared. Data points are means ± SEM of three to five replicates. Data points for macroscopic current amplitudes (a, d) are connected for clarity. For half-activation times (b, e) superimposed monoexponential decay functions are shown. For all four S4 mutants and wild type, a global fit of mean values with $z_a = 0.39 \pm 0.012$ is shown. For S10 mutants, independent fits had to be performed; for z_a values see Table 1. Data points for macroscopic conductance (c, f) were described with a Double-Boltzmann distribution with values for V_1, V_2, z_1 and z_2, as summarised in Table 1.

Table 1. Voltage-dependent gating parameters of TPC1 from *Arabidopsis thaliana*.

		activation			double-Boltzmann fit			
channel type		phases	$t_{1/2}$(80 mV)/ms	z_a	z_1	V_1/mV	z_2	V_2/mV
wild type		>1	100 ± 7.8	0.46 ± 0.01	0.9 ± 0.11	60 ± 4.6	2.7 ± 0.40	28 ± 3.0
wild type 10Ca		>1	**312 ± 39**	**~0**	0.9[a]	**156 ± 22**	2.7[a]	**73 ± 3.5**
mutants								
S4 helix	R185M	>1	128 ± 12	0.42 ± 0.02	1.2 ± 0.09	**85 ± 7.1**	3.2 ± 0.84	35 ± 2.7
	R191M	>1	101 ± 29	0.41 ± 0.06	1.2 ± 0.16	**76 ± 2.9**	2.5 ± 0.69	37 ± 5.6
	R200M	>1	87 ± 18	0.36 ± 0.01	0.8 ± 0.14	**87 ± 9.5**	2.3 ± 0.25	40 ± 4.0
	R203M	>1	80 ± 9.3	0.43 ± 0.02	1.3 ± 0.11	69 ± 5.4	2.9 ± 0.83	31 ± 3.6
S10 helix	R537M	**1**	**54 ± 4.7**	**0**	0.77 ± 0.04	**>110**		
	R540M	>1	**184 ± 11**	**0.22 ± 0.01**	0.6 ± 0.26	67 ± 22	1.6 ± 0.14	34 ± 9.9
	R543M	Hardly any SV currents at all, this mutant severely affects channel gating!						
S10–S11 linker	R550M	>1	133 ± 32	0.36 ± 0.01	1.1 ± 0.23	**94 ± 3.2**	2.6 ± 1.5	36 ± 8.1
	R552M	>1	**231 ± 48**	0.36 ± 0.01	**0.44 ± 0.03**	**147 ± 15**	2.7 ± 1.0	19 ± 3.7
Ca^{2+}-binding	E239Q	>1	**39 ± 2.2**	0.48 ± 0.07	0.73 ± 0.09	65 ± 7.6	2.4 ± 0.25	29 ± 2.7
	E239Q_10Ca	>1	**39 ± 12**	0.42 ± 0.03	0.6 ± 0.22	**79 ± 5.8**	2.1 ± 0.45	26 ± 6.8
	D454N/*fou2*	>1	**19 ± 2.6**	**0.23 ± 0.02**	0.60 ± 0.05	57 ± 11	2.8 ± 0.14	**9 ± 1.1**
	E528Q	>1	**12 ± 2.4**	0.46 ± 0.03	0.5 ± 0.1	44 ± 8.4	2.3 ± 0.14	24 ± 2.4
	E528Q_10Ca	>1	**15 ± 1.4**	0.41 ± 0.01	0.6 ± 0.1	38 ± 11	2.1 ± 0.16	**20 ± 3.2**
	R531M	**1**	**2.7 ± 0.17**	0.49 ± 0.02	0.6 ± 0.1	63 ± 14	2.4 ± 0.29	**16 ± 3.1**
	R531M_10Ca	**1**	**4.0 ± 0.93**	0.49 ± 0.02	0.65 ± 0.09	71 ± 22	2.7 ± 0.27	**17 ± 2.4**
537 partner	E450Q	>1	**25 ± 2.5**	**0.21 ± 0.05**	0.56 ± 0.011	**>110**		
	E478Q	>1	**244 ± 29**	0.45 ± 0.023	1.6 ± 0.1	**>110**		
	E511Q	>1	**56 ± 13**	0.39 ± 0.03	1.6 ± 0.1	**86 ± 7.8**	4.8 ± 5.9	30 ± 6.0

Values given indicate, from left to right, whether SV/TPC1 current activation was monoexponential or multiphasic; the half-activation time, $t_{1/2}$, at +80 mV; the slope factor for voltage dependence of half-activation times, z_a; the gating charges z_1 and z_2, defining the steepness of voltage-dependent activation; midpoint voltages for activation V_1 and V_2 (of C1 ⇄ O and C2 ⇄ C1 transition, respectively). The slope factor z_a was estimated from monoexponential fits of the voltage dependence of half-activation times (see Fig. 3). Gating charges, z_1 and z_2, and midpoint voltages for activation, V_1 and V_2, were estimated by fitting Double-Boltzmann distributions to voltage-dependent tail current amplitudes, normalised by vacuolar size. Values of best-fit parameters ± SE were calculated by global fits of three or more replicates. Where an extra sum-of-squares *F* test and Akaike's Information Criteria did not support a global fit, data sets were fitted independently and mean ± SEM of best-fit parameters given. Values in bold indicate significant differences from wild-type TPC1. Statistical significance of observed differences was determined either with a *F* test and Akaike's Information Criteria (z_a, z_1, z_2 and V_2), or by a Student's *t*-test ($t_{1/2}$, V_1).
[a]For wild type 10Ca, $z_1 = 0.9$ and $z_2 = 2.7$ were fixed to estimate V_1 and V_2 by global fits.

Double-Boltzmann distribution; they showed monoexponential voltage dependence (Fig. 3f). Apparently, a R→M substitution at position 537 caused a greater than +50 mV shift of the C1 ⇄ O closed–open transition, moving the inflection point (V_1) of conductance–voltage curves far outside the applied voltage range of up to +110 mV. Comparable current densities were monitored from vacuoles with R540M- and wild-type-TPC1 (Figs S2 and 3d). Compared to wild-type channels, R540M current activation was delayed at +80 mV by a factor of almost two. Voltage-dependence of half-activation times was also reduced by about a factor of two (Fig. 3e, Table 1). With respect to wild-type TPC1, midpoint potentials for activation (V_1 and V_2) of conductance–voltage curves from R540M were not altered (Fig. 3f, Table 1). In summary, these results are consistent with the homology model-based hypothesis that these three arginine residues act as voltage sensors.

R531M, R550M and R552M. Surrounding the three core arginines in S10 (R537, R540 and R543) are two conserved arginines at position 550 and 552 and a strictly conserved arginine at position 531 (Fig. 2). Neutralisation of the positive charge at position 550 (R550M) did not result in significant changes in half-activation times or in their voltage dependence compared to wild-type channels (Fig. 3e, Table 1). Macroscopic current densities, however, were reduced by about 35% (Figs S2 and 3d), probably due to a positive-going shift of about 34 mV in the midpoint voltage V_1 (Table 1). Compared to wild-type channels, neither the midpoint voltage V_2 nor its equivalent gating charges (z_1 and z_2) were altered in this mutant. R550M thus affected voltage gating of TPC1 in a manner comparable to arginine mutations in the S4 domain (Fig. 3c,f, Table 1). This observation is consistent with our homology model, suggesting that Arg550 is located in the S10–S11 linker region rather than constituting a part of voltage sensor helix S10.

Unexpectedly, analysis of R552M channel currents revealed a two-fold slower half-activation time compared to wild-type channels, but a comparable voltage dependence of half-activation time (Fig. 3e). Macroscopic current densities were reduced by 80% for R552M (Figs S2 and 3d), the result of a shift in the midpoint voltage V_1 by about 87 mV (Table 1). Mathematical analyses of conductance–voltage curves (Fig. 3f) indicated an approximate 50% decrease in the equivalent gating charge z_1 for the C1 ⇄ O closed–open transition. R552M was the only mutant showing a significant change in gating charge z_1, implying that Arg552 has a major voltage-sensing function. According to our model, both arginines (Arg552, Arg550) are located in the S10–S11 linker facing the cytoplasm. Whereas in our homology model the side chain of Arg550 is oriented away

from the lipid bilayer towards the cytoplasm, in our model the side chain of Arg552 faces helix S9 where it is in close proximity to Glu494. It might therefore transmit movements of the voltage sensor helix S10 to other parts of the ion channel, even though it is not an integral part of the voltage sensor helix S10.

R531M had the strongest effect of all the mutants on activation kinetics, causing a more than 30-fold acceleration of half-activation times (Figs S2 and 3e, Table 1). Nonetheless, voltage dependence of half-activation times did not differ from wild type (Table 1). Conductance–voltage curves were similar to wild-type channels (Fig. 3f), but exhibited a slightly different shape due to an approximate 10 mV reduction of the midpoint potential V_2 (Table 1). Although Arg531 is located in the voltage sensor helix S10, its side chain orientation in our model indicates that it will have little effect on voltage-dependent channel gating. Indeed, electrophysiological recordings with R531M mutants showed pronounced changes in gating kinetics, but only small effects on voltage dependence. This observation is consistent with our homology model and evolutionary analysis (Fig. 2, Table S2), suggesting that Arg531 represents an important residue for the voltage-dependent gating of TPC1.

Do Glu450 and Glu478 form ion-pairs with Arg537?

Seeking potential counter charges interacting with identified voltage-sensing arginine residues, we detected several acidic residues that could participate in channel gating. According to our homology model, Glu450 in the last turn of helix S7 and Glu511 in helix S9 was close to R3 (Arg537) and Glu478 in helix S8 to R5 (Arg543), suggesting that these oppositely charged residues may form ion pairs. We therefore analysed the voltage-dependent gating properties of channel mutants E450Q, E478Q and E511Q, which lack a negative charge. In E511Q mutants, half-activation times were accelerated about twofold (Table 1), while the voltage dependence of half-activation times was comparable to wild-type channels (Fig. 4b). Due to a positive-going shift of more than 20 mV in the midpoint voltage V_1, the current density was slightly reduced in E511Q mutants (Fig. 4a, Table 1). In summary, the voltage-dependent gating characteristics of the E511Q and the R537M mutant were rather different (Table 1), suggesting that our model might underestimate the distance between Arg537 and Glu511. In contrast, the effects of mutations E450Q and E478Q on channel gating were akin to the effects observed with the R537M mutation (Table 1). For all three mutants, a decrease in current densities was monitored (Fig. 4a). Conductance–voltage curves showed a monoexponential voltage dependence and could not be described with a Double-Boltzmann distribution (Fig. 4c). The R537M, E450Q and E478Q mutation shift the midpoint voltage V_1 to such positive voltages that the closed–closed transition (C2 ⇄ C1) hardly affects the conductance–voltage curves, and voltage-dependent gating of TPC1 is dominated by the closed–open transition (C1 ⇄ O). In summary, the characteristic and similar changes in voltage-dependent channel gating shown by our electrophysiological analyses (Fig. 4c) suggest that Glu450 and, surprisingly, Glu478 could engage with Arg537 in an ion-pairing interaction, potentially established in different conformational states during channel gating.

Arginine 531 and glutamines 528 and 239 contribute to luminal calcium sensitivity

We have previously investigated the role of negatively charged residues Asp454 and Glu450 in the S7–S8 linker. Based on this structure–function study, both residues were suggested to be part of the luminal calcium binding site (Dadacz-Narloch *et al.* 2011). The more than 30-fold acceleration of current activation observed in R531M (Fig. 3e, Table 1) resembles somewhat the pronounced acceleration of current activation found for the mutants D454N and E450Q. Binding of calcium to this luminal calcium sensor shifts both midpoint potentials, V_1 and V_2, to more positive potentials (Pottosin *et al.* 2004; Table 1), so slowing down current activation. In the mutants D454N and E450Q, the sensitivity of channel gating towards luminal calcium is lost (Beyhl *et al.* 2009; Dadacz-Narloch *et al.* 2011). A comparison of macroscopic currents measured in the virtual absence (no Ca^{2+} added) or presence of 10 mM Ca^{2+} at the luminal side of the vacuolar membrane indicates a loss of calcium sensitivity in R531M as well (Fig. S3a–c). Indeed, neither the channel activation nor voltage-dependent channel-open probability was affected by luminal calcium. These data suggest that Arg531 might be involved in connecting the luminal calcium sensor to the voltage-sensing S10 domain. However, although in our homology model Arg531 is at the luminal end of the S10 helix, so in proximity to the calcium sensor, it neither exhibits direct contact nor is its side chain oriented towards the calcium sensor. Therefore, we looked for conserved charged amino acids close to Arg531. Preceding S10, Glu528 is conserved among all land plants, and substitution of the

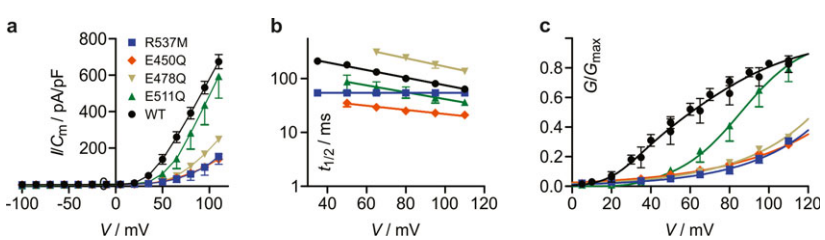

Fig. 4. Effects of mutations in potential ion partners of R537 on voltage-dependent channel gating of TPC1 from *Arabidopsis thaliana*. Two glutamate mutations (E450Q and E511Q) are compared to wild type and the arginine mutant R537M. Shown are current amplitudes (I/C_m in pA/pF; a), half-activation times ($t_{1/2}$ in ms, logarithmic *y*-axis; b) and macroscopic conductance–voltage curves (G/G_{max}; c). Data points are means ± SEM of three or more replicates. Data points for macroscopic current amplitudes (a) are connected for clarity. For half-activation times (b), superimposed monoexponential decay functions are shown. While R537M is not voltage-dependent (*i.e.* $z_a = 0$), the two glutamate mutants had slope factors z_a, similar to wild type. Data points for macroscopic conductance (c) were described using a Double-Boltzmann distribution with values for V_1, V_2, z_1 and z_2 as summarised in Table 1.

negatively charged Glu528 with glutamine resulted in channels with a gating behaviour resembling R531M: fast activation and voltage-dependent gating that is insensitive to luminal calcium (Fig. S3e,f). As with the D454N/*fou2* mutant, the loss of sensitivity towards luminal calcium seems to promote opening of E528Q and R531M mutant channels at low membrane potentials. Accordingly, D454N/*fou2*, E528Q and R531M result in higher open probabilities at membrane potentials between −30 and +30 mV (Fig. 5), likely caused by a shift of the midpoint potential V_2 to less positive voltages compared to wild type (Table 1). For E528Q, the shift in the midpoint potential V_2 is <10 mV, and is statistically supported only for recordings performed in the presence of 10 mM Ca^{2+}. For R531M, V_2 is shifted by more than 10 mV, and for D454Q/*fou2*, the shift is close to 20 mV (Table 1), resulting in several per cent open probability even at negative membrane potentials (Fig. 5). Glu239, which is at the luminal end of helix S5 of the D1 domain, was the second acidic residue that is not only conserved among all land plants, but according to our homology model, is within a 7 Å distance of Arg531 and the luminal calcium sensor. Substitution of Glu239 with glutamine resulted in fast current activation, and voltage-dependent channel gating was no longer affected by luminal calcium, resembling the mutants R531M and E528Q (Fig. S3). These results indicate that Arg531, Glu528 and Glu239 are important for the regulation of TPC1 gating by luminal calcium.

DISCUSSION

When comparing our homology model with the recently published crystal structures (Guo *et al.* 2016; Kintzer & Stroud 2016), the central channel assembly comprising helices S5 and S6 as well as the pore helices and loops superimpose very well (Fig. S4). However, both the assumed voltage paddles (S4 and S10) are shifted by several Ångstrom and tilted by some degrees. In addition, the paddle helices S4 and S10 are vertically shifted by one turn between the model and the AtTPC1 crystal structure. Thus, the position of the voltage-gating arginines in S4 and S10 as well as the prediction of potential ion pairing partner differ between our model and the crystal structure, making direct comparisons difficult. Although this difference could be due to a misalignment between the sequence of AtTPC1 and Na_vAb, it could be because in the model template, the channel Na_vAb, is in an open conformation with the voltage sensor helix in the up position (Payandeh *et al.* 2012), while the structure of AtTPC1 was determined with the channel in its closed state with the voltage sensor helix in the down position (Guo *et al.* 2016). However, as no structure is yet available for AtTPC1 in its open state, the structural differences between the model and experimental structures cannot be fully explained.

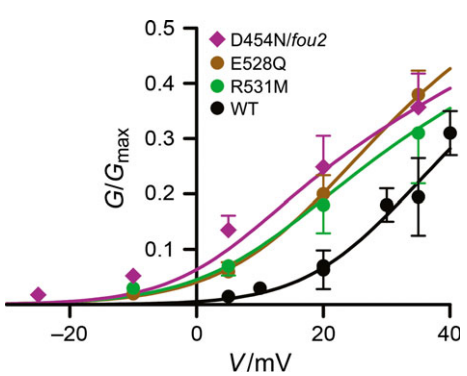

Fig. 5. Mutations resulting in higher open probabilities at less positive voltages. Macroscopic conductance–voltage curves (G/G_{max}) are compared for wild type (WT), D454N/*fou2*, E528Q and R531M from *Arabidopsis thaliana*. Data points are means ± SEM of three to five replicates. Only data points between −25 mV and +40 mV are displayed to emphasise differences in open probability ($P_O \approx G/G_{max}$) at small membrane potentials. Data points were described with a Double-Boltzmann distribution with values for V_1, V_2, z_1 and z_2 as summarised in Table 1.

Transmembrane S4 helix, a degenerated voltage paddle

Both the homology model and the crystal structure agree that helix S4 does not work as a voltage sensor. This is supported by our presented electrophysiological data from four S4 mutants, performed in the native environment of the *Arabidopsis* mesophyll vacuole. All S4 mutants display a voltage dependence similar to wild-type channels in the corresponding expression system. Of note is that in the study of Guo *et al.* (2016), the plant TPC1 was expressed in HEK cells, and in contrast to animal TPCs, the plant vacuolar two-pore channel is targeted to the plasma membrane of the animal cell rather than to the endosomal membrane as *in planta*. Interestingly, when the animal TPCs are heterologously expressed in plant cells, targeting of animal TPCs to the endosomal membrane system is maintained (Boccaccio *et al.* 2014). Comparisons between the conductance–voltage curves presented here (Figs 3–5) and the non-plant expression system in Guo *et al.* (2016) demonstrate that the voltage-dependent gating of wild-type TPC1 in HEK cells is shifted by about 60 mV to more negative membrane voltages. This distinct gating behaviour is probably caused by AtTPC1 addressed by animal TPC1 interactors (Horton *et al.* 2015; Patel 2015) that are present in HEK cells, and plant cell-atypical experimental solute compositions (cf. Pottosin *et al.* 2004). Furthermore, different post-translational modifications of plant vacuolar and animal plasma membrane proteins (Pedrazzini *et al.* 2016), the distinct protein-to-lipid ratio and lipid composition of the target membrane and/or the presence/absence of certain regulatory factors could also result in altered voltage-dependent gating of TPC1 when studied in HEK cells rather than in its native membrane.

Major voltage-sensing by transmembrane helix S10

The S10 helix in AtTPC1 displays the key signature of a voltage-sensing domain, and mutating Arg537, Arg540 or Arg543 affected the voltage gating of the TPC1 channel, as expected for a voltage sensor (Table 1). Using the crystal structure of AtTPC1, Guo *et al.* (2016) proposed a model for the voltage-gating mechanism based on these three arginine residues. Among the R→Q mutants tested by Guo *et al.* (2016), R537Q had the strongest effect. In contrast, in our study with *Arabidopsis* vacuoles, the strongest shift in the conductance–voltage curves was observed with R543M, followed by R537M and R540M (Table 1, Fig. 2). It seems possible that these different effects of S10 arginine mutations were caused by different experimental conditions. However, this does not explain why

TPC1 conductance–voltage curves observed for the HEK expression system are well described with a simple Boltzmann fit. A simple Boltzmann fit reflects a simple two-state model where the channel is either open or closed. In contrast to this, TPC1 conductance–voltage curves from intact vacuoles generally show a more complex pattern, best described using a Double-Boltzmann fit (Pottosin *et al.* 2004; Dadacz-Narloch *et al.* 2011). This is indicative of at least three states, two closed and one open channel state (C2 ↔ C1 ↔ O). Despite the higher complexity of TPC1 conformational channel states in the native membrane environment, our electrophysiological studies do indicate that in line with our model prediction and the crystal structures (Guo *et al.* 2016; Kintzer & Stroud 2016), Arg537, Arg540 and Arg543 are part of the voltage-sensing domain of TPC1. Thus, these residues serve as gating charges R3, R4 and R5, which re-orientate in response to changes in the electrical field of the vacuolar membrane.

Influence of the S10-S11 linker region on voltage gating

When Arg552, which is located in the S10–S11 linker, is replaced with methionine, gating charge and midpoint potential V_1 of the C1 ⇄ O transition were significantly changed compared to wild type (Table 1). This effect could not be explained with our homology model; the model predicted this arginine to be oriented towards the cytoplasm, thus not part of the voltage sensor helix S10. However, according to the crystal structures (Guo *et al.* 2016; Kintzer & Stroud 2016), Arg552 is in close proximity to three glutamate residues, Glu678, Glu682 and Glu685, at the C-terminal end of helix S12. We now assume that, possibly through ion pairing, Arg552 transfers vertical movements of the voltage sensor helix S10 to helix S12, which is connected to the pore helices and pore loops, thereby modulating channel opening and ion transport.

The S10 residue Arg531, a possible linker to the luminal calcium sensor

Our evolutionary studies identified Arg531, located upstream of the voltage-sensing R2 (Arg537), as one specificity-determining residue in S10 (Table S2). According to the crystal structures, Arg531 (R1) is located in the upper half of the sensor helix S10 and seems to participate in voltage sensing by engaging with Glu511 in ion-pairing (Guo *et al.* 2016; Kintzer & Stroud 2016). Accordingly, one would expect a positive-going shift in the voltage threshold for R531M activation, indicating that channel opening requires more energy and channel activation is slowed down. Instead, gating of R531M closely resembles those mutants that exhibit a defect of the luminal calcium sensor. The corresponding mutants such as D454N/*fou2* (Beyhl *et al.* 2009) are characterised by a significantly less positive midpoint potential V_2, and accelerated channel activation. Thus, channel opening in these mutants requires less energy compared to wild type (Dadacz-Narloch *et al.* 2011; Table 1). Our model and the crystal structures potentially display the different conformational states of the channel, open and closed, respectively. This corresponds to the voltage sensor helix, S10, being either in the downward or upward shifted position. Although the position of Arg531 in the open TPC1 channel is not known precisely, our electrophysiological results do suggest that at least in one conformational state, Arg531 provides a link between the voltage sensor helix, S10, and the luminal calcium sensor.

The luminal calcium sensor is located in the loop between helices S7 and S8 (Fig. 1, inset), which is in proximity to the voltage sensor helix S10. Therefore, voltage-dependent gating in TPC1 could be calcium-dependent. A first biophysical characterisation of the luminal calcium sensor postulated more than one binding site (Pottosin *et al.* 2004). Structure–function studies showed that D454N/*fou2* (Beyhl *et al.* 2009), E450Q and E457Q/N all lose sensitivity toward luminal calcium, and a homology model combined Glu450, Asp454, Glu456 and Glu457 into one calcium coordination site (Dadacz-Narloch *et al.* 2011). The crystal structure provides a picture of the luminal calcium sensor comprising two calcium coordination sites (Guo *et al.* 2016). Yet Guo *et al.* (2016) suggest that there might be only one *bona fide* calcium-binding site. The '*bona fide*' site 1 comprises Asp240 of one monomer and Asp454 and Glu528 of the other monomer. Mutants without a negative charge on any of these three calcium-coordinating side chains have been shown to lose luminal calcium sensitivity (Fig. S3; Beyhl *et al.* 2009; Dadacz-Narloch *et al.* 2011; Guo *et al.* 2016). Another potential calcium-binding site consists of Glu239 and Asp240 of one monomer and Glu457 of the other monomer. Here, results from mutant studies are less clear. Guo *et al.* (2016) report a luminal calcium sensitivity comparable to wild type for E239Q, while measurements reported here for E239Q demonstrate the loss of luminal calcium sensitivity (Fig. S2, Table 1). It is currently unclear whether this discrepancy results from different expression systems or different solution ionic composition.

Possible ion pairing of the voltage-sensing Arg537 in S10 with Glu450 and Glu478

In our homology model, which was obtained from the Na_VAb channel representing the open state, the acidic residue Glu450 forms an ion-pair with the voltage-sensing Arg537 (R3) and Asp478 pairs with Arg543 (R5). However, the crystal structure, which represents the TCP1 channel in its closed state, points to ion pairing of Arg537 with Glu478 and Asp500, while Arg543 is in close proximity to Glu494 at the beginning of helix S9 (Guo *et al.* 2016; Kintzer & Stroud 2016). Interestingly, as with the S10 helix mutant R537M, both mutants E450Q and E478Q resulted in a large shift of V_1 to more positive potentials (Table 1). The similar effects of R537M, E450Q and E478Q on channel gating can be best explained through Arg537 forming an ion pair with Glu478 when TPC1 is closed, and with Glu450 when TPC1 is in its open state. Hence, during the transition from the closed to the open channel state, helix S10 moves upward, possibly taking Arg537 away from Glu478 and bringing Arg537 in contact with Glu450. Such an upward movement of S10 is also supported by a direct comparison of the crystal structure of AtTPC1 (closed) and Na_vAb (open) (Guo *et al.* 2016; Kintzer & Stroud 2016).

CONCLUDING REMARKS

Using the native expression background, our work confirms and extends recent findings on the structure and function of the *Arabidopsis* TPC1 channel. In agreement with structural and evolutionary predictions, the transmembrane helix S10

in the D2 domain is identified as the key TPC1 voltage sensor, while the fast-evolving S4 domain in D1 appears dispensable for voltage-dependent channel gating. Among land plants, the vacuolar cation channel TPC1 is highly conserved, with 50% amino acid sequence identity between *Arabidopsis* and the moss *Physcomitrella patens*, and 61% amino acid identity between *Arabidopsis* and rice (*Oryza sativa*). Even between *Arabidopsis* and the filamentous green alga *Klebsormidium flaccidum*, which had their last common ancestor more than 500 Mya ago, 41% of amino acids in TPC1 are identical (Hori *et al.* 2014). It therefore seems reasonable to assume that the molecular mechanisms of voltage-dependent channel gating explored here for TPC1 from *Arabidopsis* can be generalised to land plants. At the same time, voltage-dependent gating of TPC1 is only definable by considering its luminal calcium sensitivity. The key residues comprising the vacuolar calcium sensor (Glu450 and Asp454) are highly conserved among TPC1 channels from land plants. Together with the existence of a common EF-hand-based cytosolic calcium sensor, this suggests that all plant TPC1 channels share a mutual regulatory mechanism that tunes channel activity to the prevailing activities of vacuolar calcium ions to that of the cytosol.

Heterologous expression of vacuolar TPC1 channels in, for example, HEK293 cells provides a means to gain mechanistic insights into biophysical properties of this channel family. However, to understand the physiological role of this channel family, particularly when considering the observed functional differences in animal *versus* plant environment, functional analyses of TPC1 in its native membrane are paramount. Future structure–function studies will benefit greatly from the TPC1 crystal structures now available (Guo *et al.* 2016; Kintzer & Stroud 2016), and will allow the dissection of the predicted contribution of this fascinating channel in local and systemic plant signalling pathways.

ACKNOWLEDGEMENTS

The study was funded by the Deutsche Forschungsgemeinschaft through FOR964 to R.H. and D.B. We thank Beata Dadacz-Narloch for help in the generation of channel mutants, the acquisition of LSM images and electrophysiological raw data.

SUPPORTING INFORMATION

Additional Supporting Information may be found online in the supporting information tab for this article:

Figure S1. Alignment of N- and C-terminal TPC1 domains.

Figure S2. Transient expression of mutated TPC1 in *tpc1-2* protoplasts.

Figure S3. Effects of mutations potentially affecting Ca^{2+} binding on voltage-dependent channel gating of TPC1.

Figure S4. Structural comparison of the 3-D homology model and the crystal structure of AtTPC1.

Table S1. Primer sequences used for introducing the point mutations into *TPC1*.

Table S2. Prediction of specificity-determining positions (SDPs) in TPC proteins.

Methods S1. Analysis of voltage-dependent channel gating.

Notes S1. Sequences of 93 land plant TPC1 proteins.

REFERENCES

Anisimova M., Gascuel O. (2006) Approximate likelihood-ratio test for branches: a fast, accurate, and powerful alternative. *Systematic Biology*, **55**, 539–552.

Beyhl D., Hörtensteiner S., Martinoia E., Farmer E.E., Fromm J., Marten I., Hedrich R. (2009) The fou2 mutation in the major vacuolar cation channel TPC1 confers tolerance to inhibitory luminal calcium. *The Plant Journal*, **58**, 715–723.

Boccaccio A., Scholz-Starke J., Hamamoto S., Larisch N., Festa M., Gutla P.V.K., Costa A., Dietrich P., Uozumi N., Carpaneto A. (2014) The phosphoinositide $PI(3,5)P_2$ mediates activation of mammalian but not plant TPC proteins: functional expression of endolysosomal channels in yeast and plant cells. *Cellular and Molecular Life Sciences*, **71**, 4275–4283.

Cang C., Bekele B., Ren D. (2014) The voltage-gated sodium channel TPC1 confers endolysosomal excitability. *Nature Chemical Biology*, **10**, 463–469.

Catterall W.A. (2010) Ion channel voltage sensors: structure, function, and pathophysiology. *Neuron*, **67**, 915–928.

Choi W.-G., Toyota M., Kim S.-H., Hilleary R., Gilroy S. (2014) Salt stress-induced Ca^{2+} waves are associated with rapid, long-distance root-to-shoot signaling in plants. *Proceedings of the National Academy of Sciences USA*, **111**, 6497–6502.

Crooks G.E., Hon G., Chandonia J.M., Brenner S.E. (2004) WebLogo: a sequence logo generator. *Genome Research*, **14**, 1188–1190.

Dadacz-Narloch B., Beyhl D., Larisch C., López-Sanjurjo E.J., Reski R., Kuchitsu K., Müller T.D., Becker D., Schönknecht G., Hedrich R. (2011) A novel calcium binding site in the slow vacuolar cation channel TPC1 senses luminal calcium levels. *The Plant Cell*, **23**, 2696–2707.

Dadacz-Narloch B., Kimura S., Kurusu T., Farmer E.E., Becker D., Kuchitsu K., Hedrich R. (2013) On the cellular site of two-pore channel TPC1 action in the Poaceae. *New Phytologist*, **200**, 663–674.

Dereeper A., Guignon V., Blanc G., Audic S., Buffet S., Chevenet F., Dufayard J.F., Guindon S., Lefort V., Lescot M., Claverie J.M., Gascuel O. (2008) Phylogeny.fr: robust phylogenetic analysis for the non-specialist. *Nucleic Acids Research*, **36**, W465–W469.

Edgar R.C. (2004) MUSCLE: a multiple sequence alignment method with reduced time and space complexity. *BMC Bioinformatics*, **5**, 113.

Finn R.D., Bateman A., Clements J., Coggill P., Eberhardt R.Y., Eddy S.R., Heger A., Hetherington K., Holm L., Mistry J., Sonnhammer E.L.L., Tate J., Punta M. (2014) Pfam: the protein families database. *Nucleic Acids Research*, **42**, D222–D230.

Furuichi T., Cunningham K.W., Muto S. (2001) A putative two pore channel AtTPC1 mediates Ca^{2+} flux in *Arabidopsis* leaf cells. *Plant and Cell Physiology*, **42**, 900–905.

Guo J., Zeng W., Chen Q., Lee C., Chen L., Yang Y., Cang C., Ren D., Jiang Y. (2016) Structure of the voltage-gated two-pore channel TPC1 from *Arabidopsis thaliana*. *Nature*, **531**, 196–201.

Hedrich R., Marten I. (2011) TPC1 – SV channels gain shape. *Molecular Plant*, **4**, 428–441.

Hedrich R., Neher E. (1987) Cytoplasmic calcium regulates voltage-dependent ion channels in plant vacuoles. *Nature*, **329**, 833–835.

Hedrich R., Flügge U.-I., Fernandez J.M. (1986) Patch-clamp studies of ion transport in isolated plant vacuoles. *FEBS Letters*, **204**, 228–232.

Hori K., Maruyama F., Fujisawa T., Togashi T., Yamamoto N., Seo M., Sato S., Yamada T., Mori H., Tajima N., Moriyama T., Ikeuchi M., Watanabe M., Wada H., Kobayashi K., Saito M., Masuda T., Sasaki-Sekimoto Y., Mashiguchi K., Awai K., Shimojima M., Masuda S., Iwai M., Nobusawa T., Narise T., Kondo S., Saito H., Sato R., Murakawa M., Ihara Y., Oshima-Yamada Y., Ohtaka K., Satoh M., Sonobe K., Ishii M., Ohtani R., Kanamori-Sato M., Honoki R., Miyazaki D., Mochizuki H., Umetsu J., Higashi K., Shibata D., Kamiya Y., Sato N., Nakamura Y., Tabata S., Ida S., Kurokawa K., Ohta H. (2014) *Klebsormidium flaccidum* genome reveals primary factors for plant terrestrial adaptation. *Nature Communications*, **5**, 3978.

Horton J.S., Wakano C.T., Speck M., Stokes A.J. (2015) Two-pore channel 1 interacts with citron kinase, regulating completion of cytokinesis. *Channels*, **9**, 21–29.

Ishibashi K., Suzuki M., Imai M. (2000) Molecular cloning of a novel form (two-repeat) protein related to voltage-gated sodium and calcium channels. *Biochemical and Biophysical Research Communications*, **270**, 370–376.

Ivashikina N., Hedrich R. (2005) K^+ currents through SV-type vacuolar channels are sensitive to elevated luminal sodium levels. *The Plant Journal*, **41**, 606–614.

Kiep V., Vadassery J., Lattke J., Maaß J.-P., Boland W., Peiter E., Mithöfer A. (2015) Systemic cytosolic Ca^{2+} elevation is activated upon wounding and herbivory in Arabidopsis. *New Phytologist*, **207**, 996–1004.

Kintzer A.F., Stroud R.M. (2016) Structure, inhibition and regulation of two-pore channel TPC1 from *Arabidopsis thaliana*. *Nature*, **531**, 258–264.

Mazin P.V., Gelfand M.S., Mironov A.A., Rakhmaninova A.B., Rubinov A.R., Russell R.B., Kalinina O.V. (2010) An automated stochastic approach to the identification of the protein specificity determinants and functional subfamilies. *Algorithms for Molecular Biology*, **5**, 1–12.

Noda M., Shimizu S., Tanabe T., Takai T., Kayano T., Ikeda T., Takahashi H., Nakayama H., Kanaoka Y., Minamino N., Kangawa K., Matsuo H., Raftery M.A., Hirose T., Inayama S., Hayashida H., Miyata T., Numa S. (1984) Primary structure of *Electrophorus electricus* sodium channel deduced from cDNA sequence. *Nature*, **312**, 121–127.

Nørholm M. (2010) A mutant Pfu DNA polymerase designed for advanced uracil-excision DNA engineering. *BMC Biotechnology*, **10**, 21.

Patel S. (2015) Function and dysfunction of two-pore channels. *Science Signaling*, **8**, re7.

Payandeh J., Scheuer T., Zheng N., Catterall W.A. (2011) The crystal structure of a voltage-gated sodium channel. *Nature*, **475**, 353–358.

Payandeh J., Gamal El-Din T.M., Scheuer T., Zheng N., Catterall W.A. (2012) Crystal structure of a voltage-gated sodium channel in two potentially inactivated states. *Nature*, **486**, 135–139.

Pedrazzini E., Caprera A., Fojadelli I., Stella A., Rocchetti A., Bassin B., Martinoia E., Vitale A. (2016) The Arabidopsis tonoplast is almost devoid of glycoproteins with complex N-glycans, unlike the rat lysosomal membrane. *Journal of Experimental Botany*, **67**, 1769–1781.

Peiter E., Maathuis F.J.M., Mills L.N., Knight H., Pelloux J., Hetherington A.M., Sanders D. (2005) The vacuolar Ca^{2+}-activated channel TPC1 regulates germination and stomatal movement. *Nature*, **434**, 404–408.

Pottosin I.I., Tikhonova L.I., Hedrich R., Schönknecht G. (1997) Slowly activating vacuolar channels cannot mediate Ca^{2+}-induced Ca^{2+} release. *The Plant Journal*, **12**, 1387–1398.

Pottosin I.I., Martínez-Estévez M., Dobrovinskaya O.R., Muñiz J., Schönknecht G. (2004) Mechanism of luminal Ca^{2+} and Mg^{2+} action on the vacuolar slowly activating channels. *Planta*, **219**, 1057–1070.

Rahman T., Cai X., Brailoiu G.C., Abood M.E., Brailoiu E., Patel S. (2014) Two-pore channels provide insight into the evolution of voltage-gated Ca^{2+} and Na^+ channels. *Science Signaling*, **7**, ra109.

Ranf S., Wunnenberg P., Lee J., Becker D., Dunkel M., Hedrich R., Scheel D., Dietrich P. (2008) Loss of the vacuolar cation channel, AtTPC1, does not impair Ca^{2+} signals induced by abiotic and biotic stresses. *The Plant Journal*, **53**, 287–299.

Schulze C., Sticht H., Meyerhoff P., Dietrich P. (2011) Differential contribution of EF-hands to the Ca^{2+}-dependent activation in the plant two-pore channel TPC1. *The Plant Journal*, **68**, 424–432.

Sheen J. (2002) A transient expression assay using Arabidopsis mesophyll protoplasts. Available from http://genetics.mgh.harvard.edu/sheenweb/protocols/AtprotoRL04.pdf (accessed 8 May 2016).

Wang X., Zhang X., Dong X.-P., Samie M., Li X., Cheng X., Goschka A., Shen D., Zhou Y., Harlow J., Zhu M.X., Clapham D.E., Ren D., Xu H. (2012) TPC proteins are phosphoinositide-activated sodium-selective ion channels in endosomes and lysosomes. *Cell*, **151**, 372–383.

Yang Z. (2007) PAML4: phylogenetic analysis by maximum likelihood. *Molecular Biology and Evolution*, **24**, 1586–1591.

Yoo S.D., Cho Y.H., Sheen J. (2007) Arabidopsis mesophyll protoplasts: a versatile cell system for transient gene expression analysis. *Nature Protocols*, **2**, 1565–1572.